Thermal conductivity evolution of a compressed expanded natural graphite – Phase change material composite after thermal cycling

Mariam Jadal, Jérôme Soto, Didier Delaunay

Version of Record: https://www.sciencedirect.com/science/article/pii/S2451904921002080
Manuscript_b007cda728dcef2fb2f0c7379f2c4574

Thermal conductivity evolution of a Compressed Expanded Natural Graphite – Phase Change Material composite after thermal cycling

Mariam JADAL[a,b] , Jérôme SOTO[a,b,*], Didier DELAUNAY[a]

[a] *Université de Nantes, CNRS, Laboratoire de Thermique et d'Energie de Nantes, UMR 6607, La Chantrerie, rue Christian Pauc, BP 50609, 44306 Nantes Cedex 3, France*
[b] *Icam Ouest, 35 avenue du Champ de Manœuvres, 44470 Carquefou, France*

* Corresponding author. Tel.: +33 2 42 52 40 52
E-mail address: jerome.soto@icam.fr

Highlights

- Thermal conductivities of CENG-PCM identical on liquid and solid phase in spite of the expansion of the plate
- Thermal conductivities and latent heat of CENG-PCM constant after 1500 melting-cooling cycles
- Delamination and deformation of CENG-PCM slab after thermal cycling
- Migration of PCM at the external surface of the CENG composite after a few thermal cycles

ABSTRACT

Compressed Expanded Natural Graphite (CENG) impregnated with Phase Change Material (PCM) is an interesting material for latent heat storage application requiring a high heat transfer rate. This composite material, that has orthotropic properties, undergoes expansion while the PCM changes phase that might affect its thermal properties and its mechanical integrity. In order to assess this possible evolution, the CENG-PCM thermal conductivities in the two principal directions have been measured before and after a 1500 thermal cycling test. The thermal characterisation was performed using two methods: a classic hot guarded plate method and a more originally inverse method. The results show no significant change of the thermal conductivity values after ageing cycles in spite of the appearance of cracks in the planar direction of the composite. We can conclude that the delamination of the CENG was not sufficient to affect the thermal conductivities. In addition, a DSC analysis shows that the latent heat is also almost unchanged after the thermal cycling.

Keywords

Latent heat storage
Phase change material
Expanded natural graphite
Thermal conductivity
Thermal cycling
Thermal characterisation

Nomenclature

C_p: thermal capacity, J K^{-1} kg^{-1}
m: mass, kg
T: temperature, °C
t: time, s
ϕ: heat transfer rate, W
ρ: density, kg m^{-3}
λ: thermal conductivity, W m^{-1} K^{-1}

Abbreviations

CENG: Compressed Expanded Natural Graphite
DSC: Differential Scanning Calorimetry
ENG: Expanded Natural Graphite
HTF: Heat Transfer Fluid
PCM: Phase Change Material
TES: Thermal Energy Storage

1. Introduction

Phase Change Materials (PCM) are frequently used for heat storage. Indeed, latent heat is a very appropriate solution for high energy density storage in a narrow temperature range or for thermal management by damping the temperature fluctuations of a medium. In addition, the heat storage temperature can be adapted by choosing the appropriated PCM. In consequence, the applications cover a wide range of domains such as solar power [1] [2], building [3–5], electronic [6–9], battery [10–13], transportation [14] [15] and industrial processes [16–19]. Unfortunately, most PCM have a low thermal conductivity (0.1-0.4 $W.m^{-1}. K^{-1}$), which limits the heat transfer rate. Several solutions exist to enhance the thermal performance [20]. One option consists in extending the exchange surface between the PCM and the surrounding medium by using a conductive structure such as fins, foams, or by encapsulating the PCM into small encapsulated samples where the Heat Transfer Fluid (HTF) flows around [21].

The Expanded Natural Graphite (ENG) is a material recurrently used as thermal conductivity enhancer for its high thermal conductive property, low cost and inert behavior even at high temperatures [22] [23]. Compressed, the ENG forms a matrix called Compressed Expanded Natural Graphite (CENG), where the PCM can stand within the materials without leaks. This shape-stabilized composite materials, CENG-PCM, gathers the thermal conductivity of the graphite matrix and the storage capacity of the PCM. The CENG matrix is manufactured by uniaxial compression of ENG. This compression leads to an orthotropic laminate structure with graphite planes parallel to the compressive plate [24]. Each layer is linked in some bonds to constitute a cohesive structure (Figure 1). This porous structure could be impregnated by capillarity with PCM to obtain the thermal conductivity enhanced PCM material.

Figure 1: Picture of a CENG-PCM composite plate.

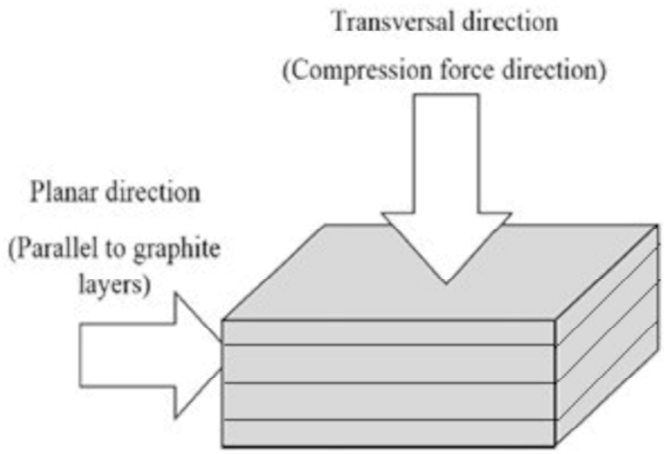

Figure 2: Different directions for calculating the thermal conductivity.

This material has been successfully applied for many applications including the waste heat recovery on industrial process [18]. Meanwhile, the tests were operated on few thermal cycles exhibited a deterioration of the matrix. Indeed, when the PCM change phases from solid to liquid, the PCM expands. This expansion induces an internal pressure within the matrix that provokes an inflation of the structure in the compressive direction, called the transverse direction (Figure 2). Therefore, we can anticipate that the thermal properties of the composite might be different in solid and in liquid phase. In addition, after multiple thermal cycles, we can expect that the structure could be deteriorated, provoking cracks and delamination and then, a decrease of the thermal conductivity.

Several authors have measured the thermal conductivity of CENG-PCM composite materials [25] [26]. However, most of time, the measures were operated when the PCM was on solid phase, and before ageing process. The purpose of this article is to measure the thermal

conductivity of a CENG-PCM composite before and after a thermal cycling ageing test, in solid and liquid phases. The thermal conductivity has been measured by two methods: an inverse method technique associated to an experimental device developed in the laboratory, and, a classic method using hot guarded plate technique. In order to achieve the inverse method, the thermal properties of the composite material, such as the phase change temperatures, the specific heat, the density and the thermal expansion were measured to be further implemented in the numerical model.

2. Thermal characterization of CENG-PCM composite before ageing test

2.1. Material

The Compressed Expanded Natural Graphite (CENG), provided by MERSEN®, has a density of 2000 kg/m^3. The CENG has been impregnated by capillarity until saturation with paraffin RT 70HC from Rubitherm®. The impregnation was performed by immersing the CENG slabs in liquid paraffin bath. To enhance, the impregnation speed, a low pressure can be imposed at the free surface of the paraffin. The CENG-PCM slabs was weighted at different times to measure the impregnation rate. After few hours, the impregnation rate reaches an asymptotic value. The mass fraction of paraffin was 80% and 20% for CENG at the end of the impregnation process.

2.2. Characterization using DSC analysis

A differential thermal analysis was carried out using a heat flux DSC, Thermal Analysis Q200. The heat flux absorbed and restored by the PCM was measured by imposing a temperature cycle on a sample of 3.5 milligrams of paraffin RT70 HC. The sample was heated from 30°C to 90°C with a constant heating rate of 8 K min^{-1}. Then, the temperature was maintained for 5 minutes to erase the thermal history of the PCM, before being cooled at the same cooling rate to reach 30°C.

From the DSC curve, we measured that the PCM starts melting at 69.5°C and the crystallization phase begins at 68.8°C (Figure 3), indicating a small supercooling of 0.7K. The enthalpy of melting and solidification, obtained from the integration of the DSC curve, was close to the value of the manufacturer data sheet: 260 kJ kg^{-1}.

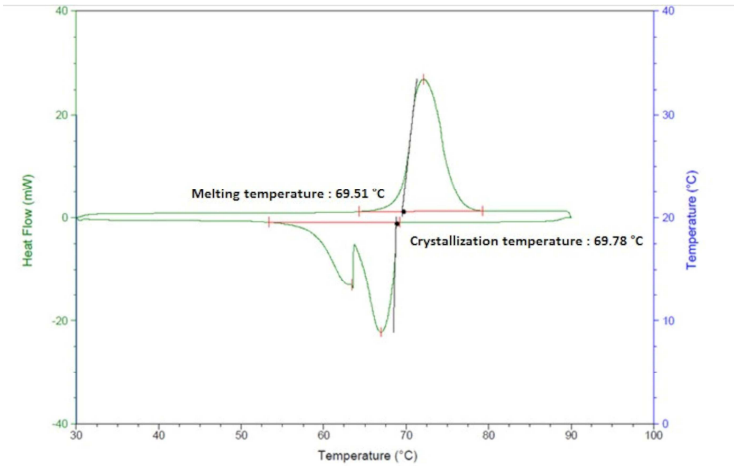

Figure 3: DSC results for RT70 HC

The specific heat, C_p, was obtained from the differential calorimetric analysis using Equation 1 (Figure 4).

$$C_p(T) = \frac{\Phi}{m.\frac{dT}{dt}} \qquad \text{Equation 1}$$

where m is the mass of the PCM sample in kg, $\frac{dT}{dt}$ the heating or cooling rate imposed by the DSC oven in K s^{-1} and Φ the heat flux measured by the DSC in W.

The average value of the specific heat of 2 000 J kg^{-1} K^{-1} was obtained in the solid phase, and of 2 200 J kg^{-1} K^{-1} in the liquid phase. In the phase change, we can observe that the apparent C_p has one peak for the melting phase and has two peaks for the crystallization phase. This singularity induces convergence problems in the numerical simulation using C_p formulation. Therefore, an enthalpy formulation has been used for heat governing equation. The enthalpy variation versus temperature is calculated by integrating the DSC curve using the Equation 2 :

$$h = \int_{T_0}^{T} C_p\,(u)\,.du + h_0 \qquad \text{Equation 2}$$

where h is the enthalpy and h_0 is a reference value of the enthalpy at the temperature T_0

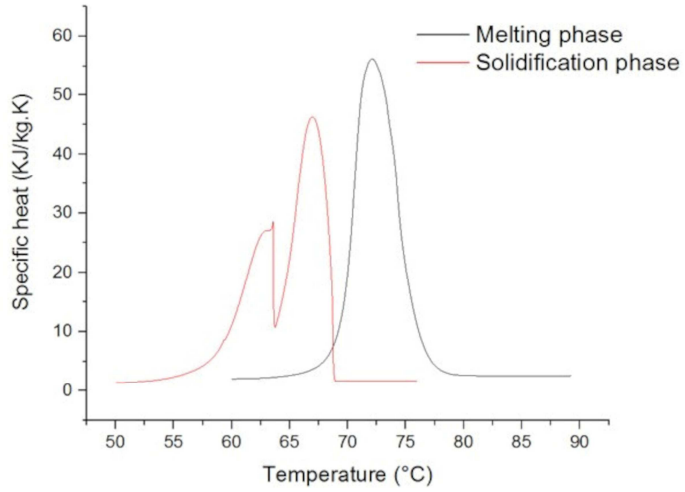

Figure 4: Apparent specific heat as a function of temperature for RT70HC obtained from the DSC at 8K min^{-1}

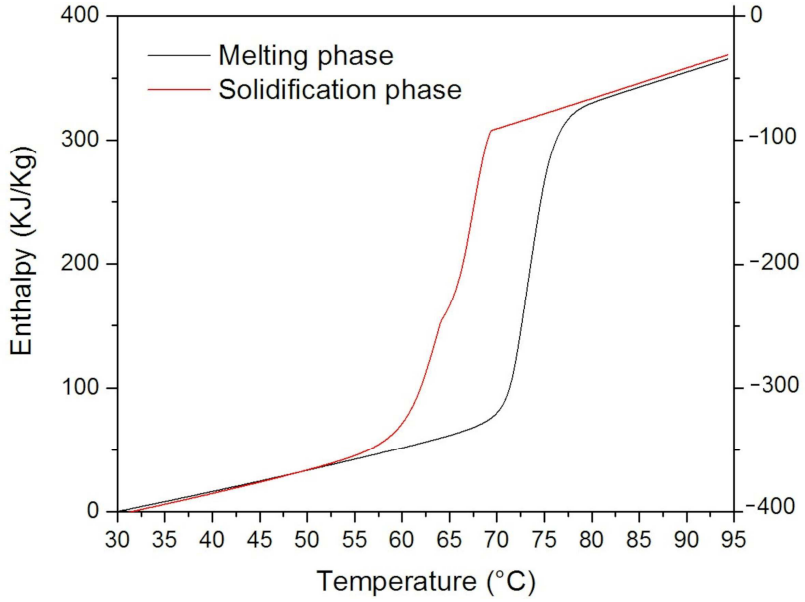

Figure 5: Apparent enthalpy as a function of temperature for RT70HC obtained from DSC analysis

The specific heat and the enthalpy evolution of GNE was also measured using the DSC. For this, a mass of 5.4 mg was taken and the same thermal cycle was imposed. Figure 6 shows the evolution of the specific heat of the GNE according to the temperature.

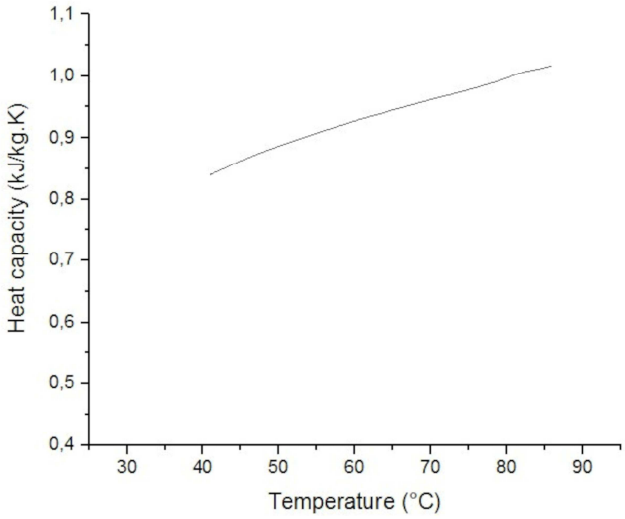

Figure 6: Specific heat according to the temperature for ENG

In the temperature range studied, from 30 to 90° C, the average value of the specific heat is 900 J kg^{-1} K^{-1}. This value is coherent with the results shown by Wang *et al* [27].

In order to determine the enthalpy *H* of the CENG-PCM, a mixing law was applied.

$$H_{GNE-MCP} = (H_{RT70\,HC}.X_{RT70\,HC}) + (H_{GNE}.X_{GNE}) \quad \text{Equation 3}$$

where X_i is the mass fraction of the material *i*.

2.3. Thermal expansion

In order to measure the thermal expansion of the composite material, two devices were utilized, namely, a PVT-alpha device [28] and a dilatometer. Their principles are based on the measurement of the thickness of the sample during an imposed thermal cycle.

At atmospheric pressure and ambient temperature, the density of the composite material was calculated by measuring the mass *m* and the volume *V* of the sample (Equation 4). A value of 878 kg m^{-3} was found.

$$\rho = \frac{m}{V} \quad \text{Equation 4}$$

The thermal expansion in both directions transverse and planar was measured by a Linseis L75 PT Horizontal Dilatometer (*Figure 7*).

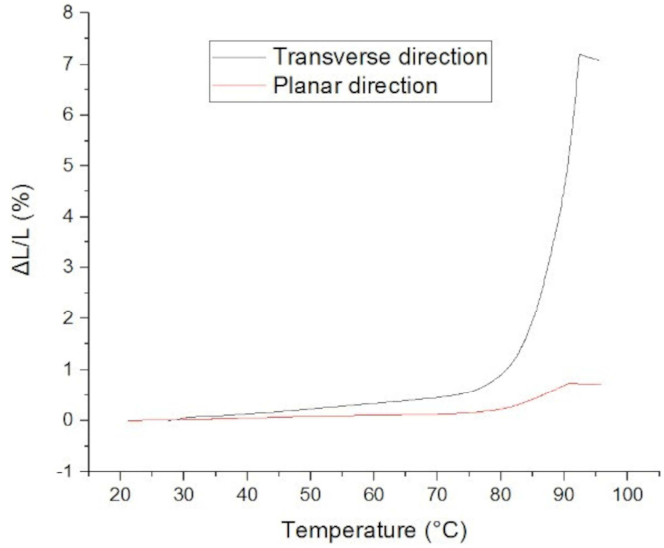

Figure 7: Planar and transverse thermal expansion of the CENG-RT70HC obtained by a dilatometer.

For a temperature range between 20 and 90°C, the thermal expansion of the material is about 8% in the transverse direction and 0.7% in the planar direction. As expected, the expansion in the transverse direction is higher than that in the planar direction, showing the orthotropy of the material.

In order to investigate if the thermal expansion and the phase change temperatures depend on the applied pressure, a test on a PVT-alpha has been performed (Figure 8).

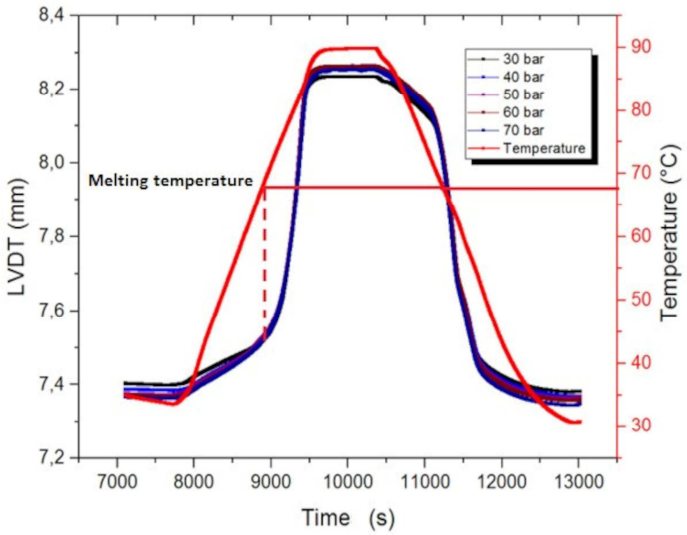

Figure 8: Transverse thermal expansion for CENG-PCM for different pressure using PVT-alpha.

The expansion evolution of the CENG-PCM does not depend significantly on the applied pressure. Therefore, we can state that the pressure does not modify the temperature phase change and the thermal expansion rate. This indicates that CENG was completely impregnated with PCM, leaving no void or air within the porous structure.

In the melting phase, we can observe that the displacement increases suddenly at the melting temperature. In a temperature range from 30 to 90° C, the thickness of the material increased by 0.7mm, representing approximately a thermal expansion of 9%. We notice the same phenomenon in the solidification phase. These values are very close to these obtained with the Linseis dilatometer.

2.4. Thermal conductivity

The thermal conductivity was measured in the planar and in the transverse directions, with two methods: a guarded hot plate and an inverse technique.

2.4.1. Guarded Hot Plate method

The thermal conductivity of the composite material was measured using a device inspired by the guarded hot plate method (Figure 9) [29]. The principle of this device is based on a unidirectional analysis of the Fourier law in stationary regime (Equation 5).

$$\phi = \lambda . S . \frac{T_{C1} - T_{C2}}{ep} \qquad \text{Equation 5}$$

with ϕ the heat flux passing through the sample, S the surface of the sample and $T_{c1} - T_{c2}$ the temperature difference between the surfaces of the sample of thickness (ep).

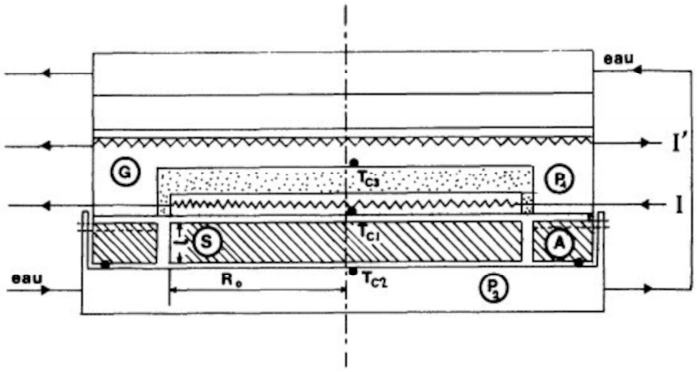

Figure 9: Guarded hot plate device [29]

Several 143mm side plates with 20mm thickness were manufactured for the thermal conductivity tests. A guard was made with the same GNE-PCM composite material to control the heat loss. The tests were carried out in the solid phase at 30°C and in the liquid phase at 90°C.

In order to measure the planar thermal conductivity with the guarded hot plate technique, the material with a thickness of 20mm, was cut into small bars. Then the plate was assembled with glue, with an orientation so that the heat flow crosses the material in its planar direction (Figure 10 and Figure 11).

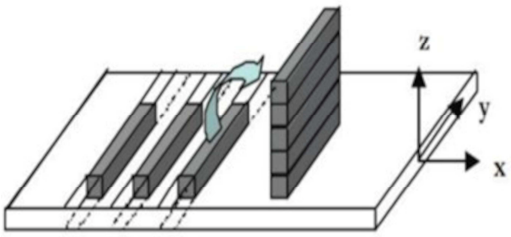

Figure 10: Sample for measurement of planar thermal conductivity [30].

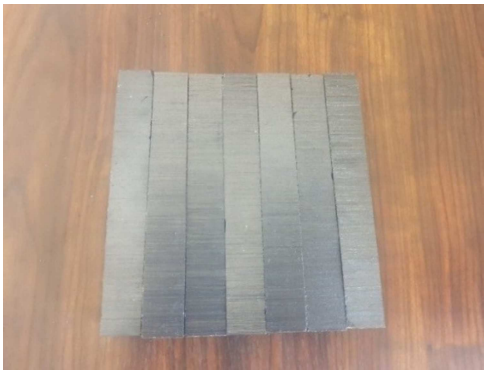

Figure 11: Composite material plate picture cut into several pieces and glued.

Table 1 shows a comparison between the values obtained for the planar and transverse thermal conductivity of CENG and the composite material in solid and liquid phases. We notice that the thermal conductivities in the transverse and planar direction are very close in the liquid and solid phase.

Table 1: Transverse and planar thermal conductivity of composite and CENG materials.

Phase	**Transverse thermal conductivity [W m^{-1} K^{-1}]**	**Planar thermal conductivity [W m^{-1} K^{-1}]**
CENG-PCM - Solid at 30°C	6.2	19.9
CENG-PCM - Liquid at 90 °C	6.4	20.2
CENG without PCM	6	20

The measurements confirm the orthotropic property of the material, since the thermal conductivity values in the planar direction strongly differ from those obtained in the transverse direction.

We notice that the thermal conductivity of the CENG plate without PCM is close to the composite sample one. This can be explained by the small value of the PCM thermal conductivity which is two orders of magnitude smaller than the graphite thermal conductivity.

2.4.2. Experimental device coupled with an inverse method

2.4.2.1. Description of the device

The test samples are identical to those used for the hot guarded plated tests. The principle of the experimental device is to impose a temperature step on one side of the plate and to measure the transient temperature distribution within the plate. The temperatures at the boundaries are set by a heat exchanger associated with thermal insulation.

A polyurethane foam was placed around this assembly to limit lateral heat losses. Two heat exchangers are placed on the upper and lower parts of the device in order to impose the initial temperature and to control the temperature at the boundaries during the tests.

The temperature at the sample edge was imposed using a piece of copper (Figure 12), where a fluid (water) circulates inside. The temperature of the water flowing within the heat exchangers and the copper part was imposed by three thermoregulators Lauda Proline RP855. In order to impose a sharp temperature variation, a bypass was installed on the fluid circuit. This also makes it possible to preheat or pre cool the fluid in a closed loop.

In order to take into account the thermal expansion of the material in the transverse direction, the thickness of the copper piece is 9% larger than the thickness of the CENG-PCM plate at solid state. A silicone seal is used to allow the thermal expansion of the material in the planar direction. The silicone seal also guarantees a uniform pressure over the sample. PTFE plates surround the sample to limit heat loss. A pressure of 0.4 bar is imposed on the upper and lower part of the plate. This pressure is sufficient to limit the thermal contact resistance without causing a damage to the plate when the PCM is liquid [31] [32].

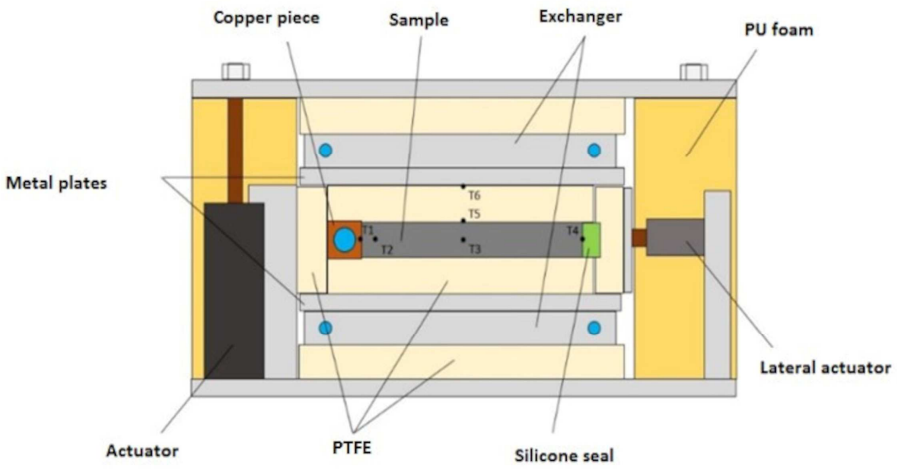

Figure 12: Experimental device for measuring planar thermal conductivity

The device is equipped with six type K thermocouples. A first thermocouple (T_1) is situated between the sample interface and the copper piece. Three thermocouples are placed at different distances from the copper piece: 10 mm (T_2), 71.5mm (T_3) and 143mm (T_4), and located in the middle of the sample. Finally, two thermocouples were also placed in both faces of PTFE plate (T_5 and T_6).

2.4.2.2. Numerical model

The 3D numerical model of the experimental device was developed using Comsol Multiphysics©. It will be used in the inverse method to identify by iteration the unknown parameters of the experiment. The governing equation implemented in Comsol is the following, where the heat equation is written with an enthalpy formulation (Equation 6):

$$\rho(T).\frac{\partial h}{\partial t} = \frac{\partial}{\partial x}\left[\lambda(T).\frac{\partial T}{\partial x}\right] \qquad \text{Equation } 6$$

Where h is the enthalpy, λ is the thermal conductivity and ρ is the density

The boundary conditions, displayed in *Figure 13*, are the following:

- A heat transfer coefficient, h, initially equal to 5 $W.m^{-2}.K^{-1}$ imposed in the lateral sides of plate, associated with the ambient temperature in the room, T_{amb}, at 23°C.
- A temperature T_6 which corresponds heat exchangers imposed temperatures
- A temperature T_1 which corresponds the copper part temperature
- A condition of symmetry in the middle plane of the plate
- Thermal resistances at interfaces between:
  - The sample and the PTFE plates
  - The sample and the copper part
  - The copper part and the PTFE plates
  - The two PTFE plates

The values of the thermal resistances and the heat transfer coefficient were updated at each iteration.

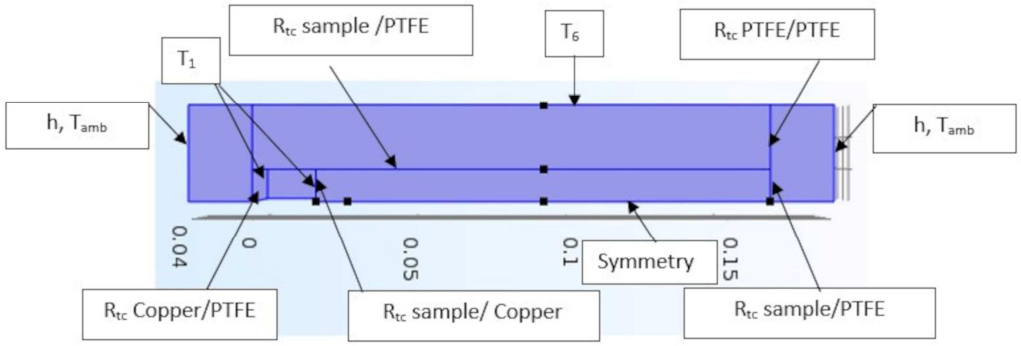

Figure 13 : Boundary conditions imposed in the numerical model

2.4.2.3. Inverse method

The inverse method consists in finding the unknown parameters by iterative method in order that the values obtained numerically fit the experimental values. The iterative method is based on the Levenberg-Marquardt algorithm [33] which consists in minimizing the function noted J calculated by Equation *7*:

$$J^i\left(R_{tc}^i, \lambda_{exp}^i\right) = \left[T_{exp} - T_{num}^i(R_{tc}^i, \lambda_{exp}^i, h_{exp}^i)\right]^T.\left[T_{exp} - T_{num}^i(R_{tc}^i, \lambda_{exp}^i, h_{exp}^i)\right] \qquad \text{Equation 7}$$

with $T_{exp}$the experimental temperature, T_{num}^{i} the numerical temperature calculated at iteration i, R_{tc}^{i} the thermals resistances and $\lambda_{\mathrm{exp}}^{\mathrm{i}}$ the thermal conductivity, $\mathrm{h}_{\mathrm{exp}}^{\mathrm{i}}$the heat transfer coefficient.

The unknown parameters to estimate by the inverse method are as follows:

- The thermal conductivity in planar direction
- The thermal resistance between the material and the copper piece
- The thermal resistance between the material and the PTFE plates
- The thermal resistance between the two PTFE plates
- The thermal resistance between the PTFE plates and the copper piece
- The heat transfer coefficient on lateral sides of the plate

For the first iteration, these parameters are imposed to an initial guessed value.

2.4.2.4. Identification of the planar thermal conductivity

i. Solid phase

In a first step, and in order to determine an initial value of the thermal contact resistance between the composite material and the PTFE plates, a transient thermal gradient in the transverse direction of the composite material was imposed by applying a uniform temperature T_6 higher that the initial temperature of the sample. The experimental temperatures T_5 and T_3 are the temperatures to fit by the numerical model in Comsol. After solving the inverse method, a value of thermal contact resistance between the composite material and the PTFE plates of 1.12 10^{-2} m^2 K W^{-1} was obtained. This value was further used as initial condition to determine the thermal conductivities.

The planar thermal conductivity identification was performed by the following procedures. The material was initially at a temperature of 24°C. A temperature of 50°C was imposed on the side of the plate T_1, using the heat transfer fluid circulating inside the copper piece. In the 3D numerical model, these experimental conditions were simulated by imposing the evolution of temperature T_1 as a boundary condition. A temperature T_6 of 24°C was set at the upper and lower PTFE plates. The initial value of the heat transfer coefficient of 5 W m^{-2} K^{-1}, associated with an ambient temperature of 25°C was imposed for the lateral boundary conditions of the assembly. The Table 2 shows the results found by inverse method.

Table 2: Inverse method results in solid phase.

Parameters	Values
Planar thermal conductivity	20.3 W m^{-1} K^{-1}
Thermal contact resistance between the sample and the copper part	1.7 x 10^{-4} m^2 K W^{-1}
Thermal resistance between sample and PTFE plate	1.6 x 10^{-2} m^2 K W^{-1}
Thermal contact resistance between copper part and	1.5 x 10^{-3} m^2 K W^{-1}

PTFE plate	
Thermal contact resistance between two PTFE plates	2.5×10^{-6} m^2 K W^{-1}
Heat transfer coefficient at the lateral plates	1 W m^{-2} K^{-1}

In order to check the validity of the final values identified using the inverse method a comparison between the temperatures T_2 and T_3 obtained experimentally and numerically, are plotted in Figure 14.

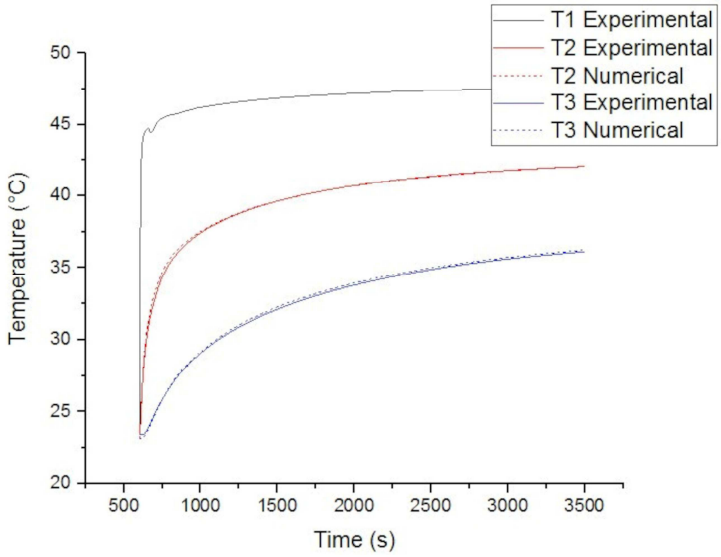

Figure 14: Temperatures T_2 and T_3 obtained experimentally and numerically in solid phase

The numerical results compared to the experimental measurements show a very good agreement, with a calculated least square difference of 0.01 K. This difference is of the order of magnitude of the accuracy of the measure and thus confirms the values obtained.

The planar thermal conductivity value obtained by the inverse method is very close to the measurements of the guarded hot plate device. The results also showed that the thermal resistance value between the copper and the sample obtained is very low, indicating to a good contact, with 0.4 bar pressure applied. We have also observed that the thermal contact resistance between the sample and the PTFE plate obtained in the first and second stages are very close.

ii. Liquid phase

In this part, only the planar thermal conductivity, and the thermal contact resistances between the sample and the copper piece, and between the sample and the PTFE plate will be recalculated in the liquid phase. It was assumed that the other parameters do not change according to the physical state of the material. The thermal conductivity was determined here in liquid phase, for two configurations: by heating the composite from 82°C to 90°C and by cooling it from 92°C to 80°C.

The results of the inverse method are presented in *Table 3*.

Table 3: Inverse method results in heating and cooling the composite material in the liquid phase.

	Heating	**Cooling**
Planar thermal conductivity [W m^{-1} K^{-1}]	20.9	20.9
Thermal contact resistance between copper part and the sample [m^2 K W^{-1}]	9.4 x 10^{-5}	9.1 x 10^{-5}
Thermal resistance between the sample and the PTFE plate [m^2 K W^{-1}]	2.7 x 10^{-5}	6.7 x 10^{-4}

The results obtained by inverse method, were implemented in the direct model to compare numerical and experimental results (Figure 15).

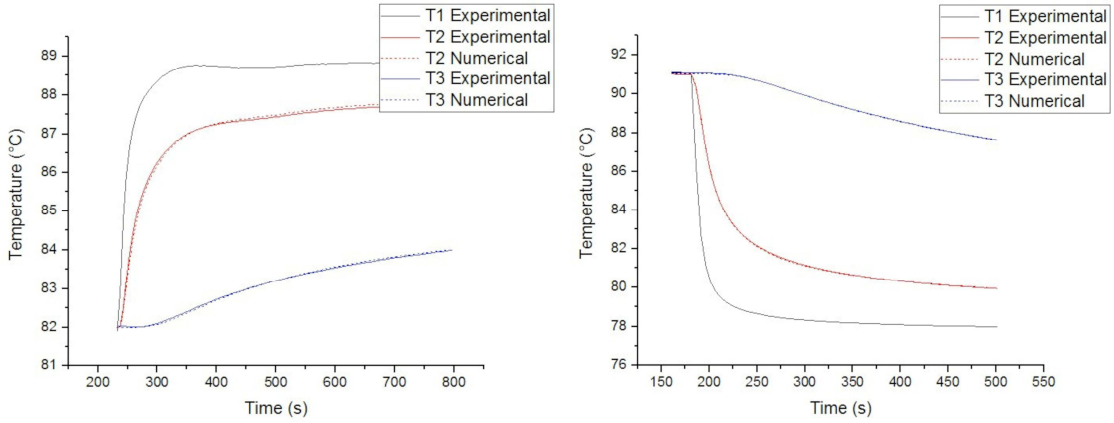

Figure 15: Temperatures T_2 and T_3 obtained experimentally and numerically in liquid phase in heating (left) and cooling (right)

The curves show a very good agreement between the experimental and numerical results for these parameters. It is established that the parameters identified by inverse method in liquid phase, in heating and cooling, are identical. The thermal conductivity values in liquid phase are also very close to those obtained using the guarded hot plate device.

3. Ageing study of a composite material plate

3.1. Experimental device

A modified version of the previously experimental device was used, allowing an automatic heating and cooling of composite material plate on one of its faces (*Figure 16*). The heat transfer then takes place in the transverse direction, which is not the most favorable case compared to heating in the planar direction. However, this drawback is compensated by a larger heat exchange surface. A PTFE plate with a PT100 probe is located below the composite material in order to estimate the temperature in the thickness of the CENG-PCM material. To limit heat losses, PTFE plates are used on all sides of the sample.

Four actuators apply a pressure on the plate to ensure a good contact between the sample and the heat exchanger plate. The actuators apply a pressure of 0.4 bars.

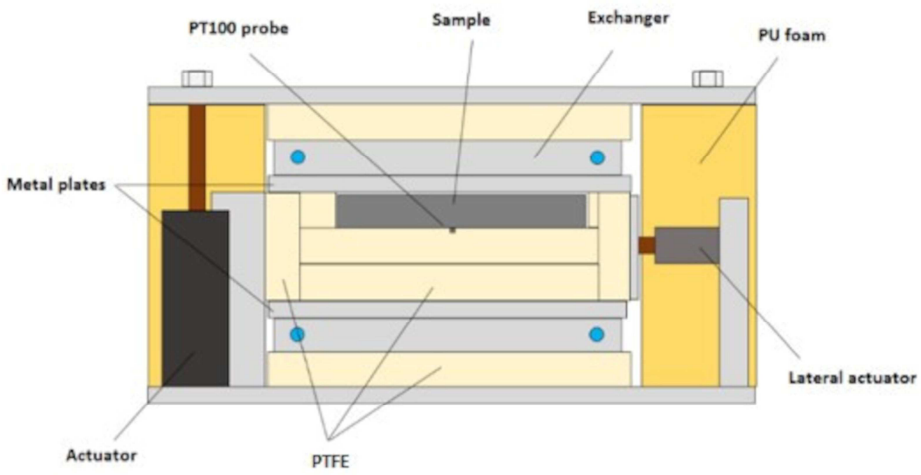

Figure 16: Ageing device picture.

The heat exchangers impose a thermal heating and cooling cycle with 1 K.min^{-1} heating and cooling rate. This rate corresponds to the maximum achievable value taking into account the inertia of the system and the heating rate capacity of the thermo-regulator (Lauda Proline RP855).

During the heating process, the Lauda set point temperature was fixed at 90°C. When the temperature of the face opposite to the heating of the composite plate indicated by the Pt100 probe, reaches 80°C, the temperature is maintained for 3 minutes before starting the cooling cycle. During cooling step, the Lauda set point temperature was fixed at 54°C. Once the temperature of the opposite side to cool reaches 55°C, the temperature was maintained for 3 minutes before switching to the heating cycle.

3.2. Experimental results

1500 thermal cycles were imposed on the sample. Each cycle lasted around 83 minutes. Figure 17 shows the typical shape of the evolution of the temperature in the sample indicated by the Pt100 according to time for ten thermal cycles.

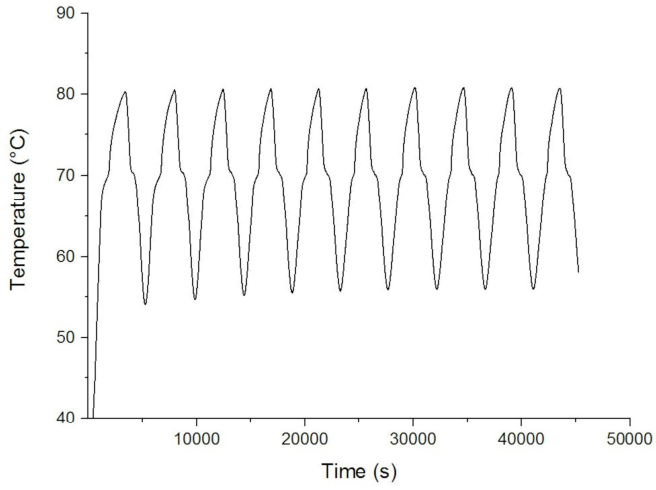

Figure 17: Temperature of the composite material on the opposite face of the exchanger, according to time during thermal cycling test

During the cycles, we noticed a warpage of the composite material on the transverse direction with a curvature of the plate Figure 18 in spite of the pressure imposed by the actuators. This warpage is due to the mechanical stresses occurring during the solidification of the material. Indeed, unilateral cooling generates a thermal gradient in the thickness of the plate, causing a differential shrinkage during the solidification.

Figure 18 shows the plate deformed during the first cycles. A maximum deflection of the edges of 2 millimeters was observed.

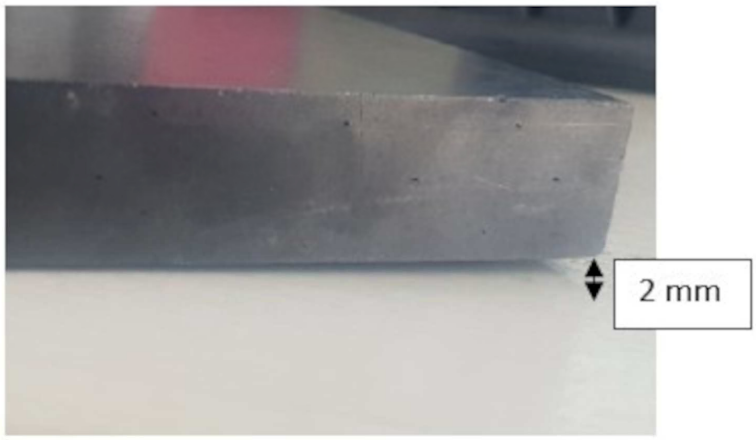

Figure 18: Composite material picture deformed after 2 cycles.

This warpage caused contact problems between the sample and the heat exchanger. Thus, an additional thermal resistance hinders the heat flow imposed by the exchanger.

After 1500 cycles, we observed a migration of the paraffin at the upper and lower surfaces of the plate (Figure 19). A loss of mass of 4% was measured. The amount of lost mass depends on the pressure applied to the slab. Indeed, during the phase change, the slab thickness increases due to the internal pressure imposed by the paraffin volume expansion when melting. When the external pressure applied to the surface of the slab is higher than the internal pressure, the slab thickness stops to freely increase, and the paraffin moves out of the CENG. The paraffin moves from the sides to the upper and lower surfaces of the slab where a free space appears due to the deformation of the slab. This migration appeared on the surface of the plate, during the first cycle and was stabilized after the 4^{th} cycle.

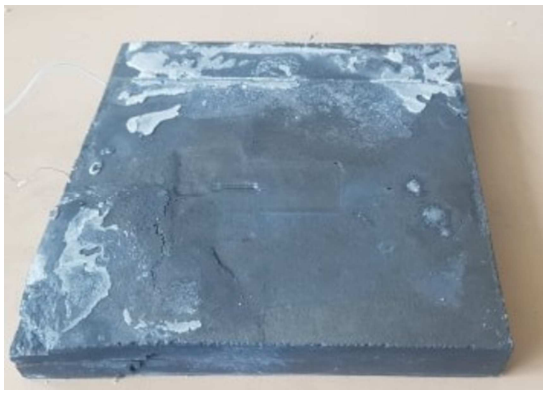

Figure 19: Appearance of paraffin on the surface of the material after 1500 cycles.

Figure 20: Cracks in the composite material after ageing.

As expected, we noticed cracks in the planar direction of the composite material (*Figure 20*) that could lead to a delamination of the plate.

3.3. Identification of thermal properties after ageing process

3.3.1. Thermal conductivity

3.3.1.1. Guarded hot plate device

The thermal conductivity in planar and transverse directions was obtained before and after the cycling by using the inverse method and the guarded hot plat device was performed. In the solid and liquid phase, the temperature of the composite material was respectively set at 30°C and 90°C. Then, for each case, the thermal conductivity was calculated (Table 1).

Table 1: Transverse thermal conductivity before and after the cycling of material in solid and liquid phases.

	Solid phase [W m^{-1} K^{-1}]	**Liquid phase [W m^{-1} K^{-1}]**
Before cycling	6.2	6.4
After cycling	6.1	6.4

The results show that the thermal conductivity in the transverse direction of the composite material before and after cycling are almost identical, despite the appearance of the cracks

3.3.1.2. Experimental device coupled with inverse method

The thermal conductivities have been calculated in solid and fluid phases. For solid phase, the plate was heated from 27°C to 50°C and from 82°C to 92°C in liquid phase. The results are displayed in Table 2.

Table 2: Thermal properties before and after cycling.

	Solid phase		**Liquid phase**	
	Before cycling	**After cycling**	**Before cycling**	**After cycling**

Planar thermal conductivity [W m^{-1} K^{-1}]	20.3	20.7	20.9	20.8
Thermal resistance between sample and PTFE plate [m^2.K.W^{-1}]	0.016	0.08	2.7×10^{-5}	4.9×10^{-2}

The results show that the value of the planar thermal conductivity is almost identical after 1500 cycles. However, an increase in the values of thermal contact resistance has been observed. Thus, as expected, the thermal resistance between the sample and the PTFE plates increased, due to the warpage of the plate. This deformation created an air gap between the sample and the PTFE plate.

Unexpectedly, the diminution of the thermal conductivities due to CENG structure deterioration was not observed. This can be explained by the ageing process that keeps a pressure on the slab during the whole time. Therefore, the delamination appears only on few millimeters from the sides of the slab. In consequence, the average value of the transverse thermal conductivity does not change significantly. The result might be different with a small sample or with a different ageing process.

3.3.2. Latent heat and phase change temperature

A DSC analysis was performed on a paraffin sample collected at the surface of the CENG-PCM plate that migrated outside (*Figure 21*). The sample is a mixture between paraffin and graphite powder with a majority of paraffin.

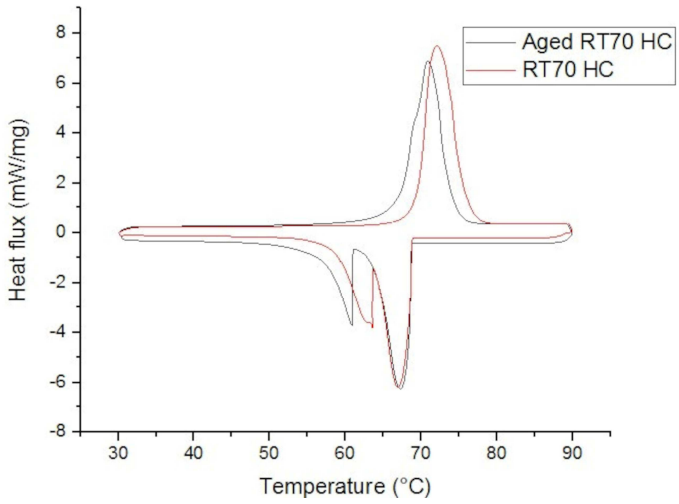

Figure 21: DSC for before and after ageing RT70 HC

The latent heat is 251 KJ kg^{-1} after ageing. This value is very close to the paraffin before ageing (260 kJ.kg^{-1}). However, graphite particles were observed in the aged sample tested. This negatively influences enthalpy value. We can therefore conclude that the loss of storage capacity is less than 3%. This confirms the work showing that the thermal storage capacity are not affected significantly by thermal cycling [34] [35]. Similarly, the phase change

temperatures remained the same. The paraffin starts solidifying at 68.7°C after ageing and 68.8°C before ageing. However, the onset melting temperature starts at 68.4°C after ageing and 69.5°C before ageing. This temperature difference is probably due to the degradation of the PCM leading to the decrease of the molecule length. The modification of the kinetic during ageing will be investigated in future publication.

4. Conclusion

The thermal characterization of a phase change material impregnated in a conductive structure based on expanded natural graphite has been carried out. The thermal properties of the material have been identified in the solid and liquid phase of the PCM material. The phase change temperatures and the specific heat capacity were identified using a DSC analysis. The planar and transverse thermal conductivities of the composite material were identified using a guarded hot plate device and an inverse method.

A study of the ageing of composite material was carried out in order to observe the effect of 1500 thermal cycles. In addition to warpage, paraffin migration on the upper and lower surfaces of the GNE plate appeared after cycling. The thermal conductivities of the aged plate were calculated using both methods showing identical values before and after cycling.

As a result, we can state that, the thermal conductivity is not affected by the thermal cycling in spite of the appearance of cracks. The delamination was probably not sufficient to deteriorate the thermal performance. The identical values of thermal conductivities found in solid or liquid phases also reveal that the expansion of the CENG gives no consequence. In addition, the latent heat remained constant after 1500 cycles showing a good thermal stability of the CENG-RT70HC material.

Acknowledgements

The authors want to acknowledge Nicolas LEFEVRE, Arnaud ARRIVE and Julien AUBRIL for their technical support.

Funding

This work was supported by the ERDF CIPITAP programme 2014-2020 Pays de la Loire, by the French Environment and Energy Management Agency ADEME and the Pays de la Loire Region.

References

[1] B. Stutz, N. Le Pierres, F. Kuznik, K. Johannes, E. Palomo Del Barrio, J.-P. Bédécarrats, S. Gibout, P. Marty, L. Zalewski, J. Soto, N. Mazet, R. Olives, J.-J. Bezian, D.P. Minh, Storage of thermal solar energy, Comptes Rendus Phys. 18 (2017). https://doi.org/10.1016/j.crhy.2017.09.008.

[2] B. Xu, P. Li, C. Chan, Application of phase change materials for thermal energy storage in concentrated solar thermal power plants: A review to recent developments, Appl. Energy. 160 (2015) 286–307. https://doi.org/10.1016/j.apenergy.2015.09.016.

[3] J.M.P.Q. Delgado, J.C. Martinho, A. Vaz Sá, A.S. Guimarães, V. Abrantes, Thermal Energy Storage with Phase Change Materials, A Literature Review of Applications for Buildings Materials, 2019. https://doi.org/10.1007/978-3-319-97499-6.

[4] F. Kuznik, D. David, K. Johannes, J.J. Roux, A review on phase change materials integrated in building walls, Renew. Sustain. Energy Rev. 15 (2011) 379–391. https://doi.org/10.1016/j.rser.2010.08.019.

[5] L.F. Cabeza, a. Castell, C. Barreneche, a. De Gracia, a. I. Fernández, Materials used as PCM in thermal energy storage in buildings: A review, Renew. Sustain. Energy Rev. 15 (2011) 1675–1695. https://doi.org/10.1016/j.rser.2010.11.018.

[6] Q. Ren, P. Guo, J. Zhu, International Journal of Heat and Mass Transfer Thermal management of electronic devices using pin-fin based cascade microencapsulated PCM / expanded graphite composite, 149 (2020) 1–16. https://doi.org/10.1016/j.ijheatmasstransfer.2019.119199.

[7] H. Muhammad, A. Arshad, M. Jabbal, P.G. Verdin, International Journal of Heat and Mass Transfer Thermal management of electronics devices with PCMs filled pin-fin heat sinks : A comparison, Int. J. Heat Mass Transf. 117 (2018) 1199–1204. https://doi.org/10.1016/j.ijheatmasstransfer.2017.10.065.

[8] S. Kumar, M.K. Das, P. Rath, Application of TCE-PCM based heat sinks for cooling of electronic components : A review, Elsevier, 2016. https://doi.org/10.1016/j.rser.2015.12.238.

[9] Z. Ling, Z. Zhang, G. Shi, X. Fang, L. Wang, X. Gao, Y. Fang, T. Xu, S. Wang, X. Liu, Review on thermal management systems using phase change materials for electronic components , Li-ion batteries and photovoltaic modules, Renew. Sustain. Energy Rev. 31 (2014) 427–438. https://doi.org/10.1016/j.rser.2013.12.017.

[10] S. Landini, J. Leworthy, T.S. O'Donovan, A Review of Phase Change Materials for the Thermal Management and Isothermalisation of Lithium-Ion Cells, J. Energy Storage. 25 (2019) 100887. https://doi.org/10.1016/j.est.2019.100887.

[11] H. Fathabadi, High thermal performance lithium-ion battery pack including hybrid active-passive thermal management system for using in hybrid/electric vehicles, Energy. 70 (2014) 529–538. https://doi.org/10.1016/j.energy.2014.04.046.

[12] Y. Lv, X. Yang, G. Zhang, Durability of phase-change-material module and its relieving effect on battery deterioration during long-term cycles, Appl. Therm. Eng. 179 (2020) 115747. https://doi.org/10.1016/j.applthermaleng.2020.115747.

[13] Y. Lv, G. Liu, G. Zhang, X. Yang, A novel thermal management structure using serpentine phase change material coupled with forced air convection for cylindrical battery modules, J. Power Sources. 468 (2020) 228398. https://doi.org/10.1016/j.jpowsour.2020.228398.

[14] J. Jaguemont, N. Omar, P. Van den Bossche, J. Mierlo, Phase-change materials (PCM) for automotive applications: A review, Appl. Therm. Eng. 132 (2018) 308–320. https://doi.org/10.1016/j.applthermaleng.2017.12.097.

[15] M. Gumus, Reducing cold-start emission from internal combustion engines by means of thermal energy storage system, Appl. Therm. Eng. 29 (2009) 652–660. https://doi.org/10.1016/j.applthermaleng.2008.03.044.

[16] P. Royo, L. Acevedo, V.J. Ferreira, T. García-Armingol, A.M. López-Sabirón, G. Ferreira, High-temperature PCM-based thermal energy storage for industrial furnaces installed in energy-intensive industries, Energy. 173 (2019) 1030–1040.

https://doi.org/10.1016/j.energy.2019.02.118.

[17] L. Miró, J. Gasia, L.F. Cabeza, Thermal energy storage (TES) for industrial waste heat (IWH) recovery: A review, Appl. Energy. 179 (2016) 284–301. https://doi.org/10.1016/j.apenergy.2016.06.147.

[18] K. Merlin, J. Soto, D. Delaunay, L. Traonvouez, Industrial waste heat recovery using an enhanced conductivity latent heat thermal energy storage, Appl. Energy. 183 (2016) 491–503. https://doi.org/10.1016/j.apenergy.2016.09.007.

[19] H. Xu, W.Y. Lin, F. Dal Magro, T. Li, X. Py, A. Romagnoli, Towards higher energy efficiency in future waste-to-energy plants with novel latent heat storage-based thermal buffer system, Renew. Sustain. Energy Rev. 112 (2019) 324–337. https://doi.org/10.1016/j.rser.2019.05.009.

[20] Y.B. Tao, Y. He, A review of phase change material and performance enhancement method for latent heat storage system, 93 (2018) 245–259.

[21] P.B. Salunkhe, P.S. Shembekar, A review on effect of phase change material encapsulation on the thermal performance of a system, Renew. Sustain. Energy Rev. 16 (2012) 5603–5616. https://doi.org/10.1016/j.rser.2012.05.037.

[22] S. Pincemin, R. Olives, X. Py, M. Christ, Highly conductive composites made of phase change materials and graphite for thermal storage, Sol. Energy Mater. Sol. Cells. 92 (2008) 603–613. https://doi.org/10.1016/j.solmat.2007.11.010.

[23] N. Calvet, X. Py, R. Olivès, J.P. Bédécarrats, J.P. Dumas, F. Jay, Enhanced performances of macro-encapsulated phase change materials (PCMs) by intensification of the internal effective thermal conductivity, Energy. 55 (2013) 956–964. https://doi.org/10.1016/j.energy.2013.03.078.

[24] X. Py, R. Olives, S. Mauran, Paraffin/porous-graphite-matrix composite as a high and constant power thermal storage material, Int. J. Heat Mass Transf. 44 (2001) 2727–2737.

[25] Y. Zhong, S. Li, X. Wei, Z. Liu, Q. Guo, J. Shi, L. Liu, Heat transfer enhancement of paraffin wax using compressed expanded natural graphite for thermal energy storage, Carbon N. Y. 48 (2010) 300–304. https://doi.org/10.1016/j.carbon.2009.09.033.

[26] D. Haillot, F. Nepveu, V. Goetz, X. Py, M. Benabdelkarim, High performance storage composite for the enhancement of solar domestic hot water systems. Part 2: Numerical system analysis, Sol. Energy. 86 (2012) 64–77. https://doi.org/10.1016/j.solener.2011.09.006.

[27] Z.T. L. Wange, S. Metcalf, R.E. Critoph, R. Thorpe, Thermal conductivity and permeability of consolidated expanded naturel graphite teated with sulphuric acid, ELSEVIER. 49 (2011) 4812–4819.

[28] BOYARD N., MILLISCHER A., SOBOTKA V., BAILLEUL J-L., DELAUNAY D., Behaviour of a moulded composite part: modelling of dilatometric curve (constant pressure) or pressure (constant volume) with temperature and conversion degree gradients, Compos. Sci. Technol. 67 (2007) 943–954.

[29] D. Delaunay, P. Carré, Dispositif de mesure automatique de la conductivité thermique des matériaux à changement de phase, Rev. Phys. Appliquée. 17 (1982) 209–215. https://doi.org/10.1051/rphysap:01982001704020900.

[30] J. FARAJ, Analyse thermocinétique de la cristallisation en milieu confiné d'un composite à base d'une résine thermoplastique (Polyamide 66), Thèse de doctorat, Université de Nantes, 2016.

[31] K. Merlin, Caractérisation thermique d'un matériau à changement de phase dans une structure conductrice, (2016).

[32] M. Jadal, K. Merlin, Didier Delaunay, Lingai Luo, J. Soto, Etude d'un dispositif de caractérisation thermique de matériaux composites : application à un matériau à changement de phase dans une structure conductrice, in: Compte Rendu Du Congrès La Société Française La Therm. SFT, Marseille, 2016.

[33] D. Maillet, M. Sablier, Spectrométrie de en masse - Principe Problèmes inverses diffusion thermique - Formulation et résolution du et appareillage problème des moindres carrés Par : Problèmes inverses en diffusion thermique Formulation et résolution du problème des moindres carr, (2015).

[34] M. K. Rathod and J. Banerjee, Thermal stability of phase change materials used in latent heat energy storage systems: A review, Renew. Sustain. Energy Rev. 18 (2013) 246–258. https://doi.org/10.1016/j.rser.2012.10.022.

[35] Z. Huang, Z. Luo, X. Gao, X. Fang, Y. Fang, Investigations on the thermal stability, long-term reliability of LiNO3/KCl – expanded graphite composite as industrial waste heat storage material and its corrosion properties with metals, Appl. Energy. 188 (2017) 521–528. https://doi.org/10.1016/j.apenergy.2016.12.010.